Mon. Not. R. Astron. Soc. **000**, 1–?? (0000) Printed 17 March 2024 (MN LATEX style file v2.2)

# *AstroSat* view of LMC X-2: Evolution of broadband X-ray spectral properties along a complete Z-track

V. K. Agrawal⋆, Anuj Nandi
*Space Astronomy Group, ISITE Campus, U. R. Rao Satellite Center, Bangalore, 560037, India*

arXiv:2007.05938v2 [astro-ph.HE] 21 Jul 2020

17 March 2024

**ABSTRACT**

In this paper, we report the first results of the extragalactic Z-source LMC X-2 obtained using the $\sim$ 140 ks observations with *Large Area X-ray Proportional Counter (LAXPC)* and *Soft X-ray Telescope (SXT)* onboard *AstroSat*. The HID created with the *LAXPC* data revealed a complete Z-pattern of the source, showing all the three branches. We studied the evolution of the broadband X-ray spectra in the energy range of $0.5 - 20.0$ keV along the Z-track, a first such study of this source. The X-ray spectra of the different parts of the Z-pattern were well described by an absorbed Comptonized component. An absence of the accretion disc component suggests that the disc is most probably obscured by a Comptonized region. The best fit electron temperature ($kT_e$) was found to be in the range of $1.7 - 2.1$ keV and optical depth ($\tau$) was found to be in the range of $13.2 - 17.5$. The optical depth ($\tau$) increased as the source moved from the normal/flaring branch (NB/FB) vertex to the upper part of the FB, suggesting a possible outflow triggered by a strong radiation pressure. The power density spectra (PDS) of HB and NB could be fitted with a pure power-law of index $\alpha \sim 1.68$ and 0.83 respectively. We also found a weak evidence of QPO ($2.8\ \sigma$) in the FB. The intrinsic luminosity of the source varied between $(1.03 - 1.79) \times 10^{38}$ ergs/s. We discuss our results by comparing with other Z-sources and the previous observations of LMC X-2.

**Key words:** accretion, accretion discs - X-rays: binaries - X-rays: individual: LMC X-2

## 1 INTRODUCTION

Low mass X-ray binaries (LMXBs) are systems where a compact object accretes matter from a low mass companion ($\leqslant 1\ M_{\odot}$) via Roche lobe overflow. LMXBs hosting a low-magnetic field neutron star provide an ideal laboratory to study the physics of accretion processes at the vicinity of an ultra dense compact object and in the strong gravity regime. Early studies of the selected bright LMXBs revealed that the six luminous LMXBs trace an approximate Z-type pattern in the Colour-Colour Diagram (CCD) and the Hardness-Intensity Diagram (HID), and hence they were named Z-sources (Hasinger and van der Klis 1989). The three branches of the Z-track are: horizontal branch (HB), normal branch (NB) and flaring branch (FB). They are the brightest X-ray binaries, accreting close to the Eddington limit ($0.5 - 1.0\ L_{Edd}$). The other class of the neutron star LMXBs exhibited a fragmented pattern in the CCD and HID, and are termed as atoll sources (Hasinger and van der Klis 1989). Luminosities of these sources vary in a wider range ($0.01 - 0.2\ L_{Edd}$).

X-ray spectra of Z-sources in the $0.5 - 30$ keV range are described by two component models. The soft component is either modeled by a multi-colour disc (MCD) (*diskbb* in XSPEC) emission (Mitsuda et al. 1984; Di Salvo et al. 2002; Agrawal and Sreekumar 2003; Agrawal and Misra 2009) or a single temperature blackbody (*bbody* in XSPEC) (Di Salvo et al. 2000; Di Salvo et al. 2001). The hard component is described by a Comptonized component (*compTT* or *nthComp* in XSPEC), resulting from the inverse-Compton scattering of the soft seed photons. A combination *diskbb+bbody* is also frequently used to model the X-ray spectra of many bright LMXBs (Cackett et al. 2010; Lin et al. 2012). A combination *cutoff-powerlaw+bbody* is also some time used to describe the spectra of Z-sources (Balucinska-Church et al. 2010; Jackson et al. 2009).

Detailed studies have been carried out in order to understand the evolution of the X-ray spectra along the Z-track (Cyg X-2: Di Salvo et al. 2002; Balucinska-Church et al. 2010; Done, Zycki and Smith 2002; Farinelli et al. 2009,

⋆ E-mail: vivekag@ursc.gov.in

GX 17+2: Agrawal et al. 2020; Di Salvo et al. 2000; Lin et al. 2012, GX 349+2: Agrawal and Sreekumar 2003; Sco X-1: Church et al. 2012; GX 5-1: Jackson et al. 2009; Bhulla et al. 2019, GX 340+0: Iaria et al. 2006). Z-sources also show Quasi-periodic Oscillations (QPOs) in the range of $5-1200$ Hz (for review, see van der Klis 2000). Three types of QPOs, horizontal branch oscillations (HBOs, $15-100$ Hz), normal/flaring branch oscillations (N/FBOs, $5-30$ Hz) and a pair of kHz QPOs ($200-1200$ Hz) have been reported in the Z-sources.

LMC X-2 is one of the brightest low mass X-ray binaries in the Large Magellanic Cloud (LMC). The optical counter-part of this source is a variable $18^{\rm th}$ mag blue star (Pakull 1978). The source is reported to have persistent nature with X-ray luminosity varying in a narrow range of $0.6-3\times10^{38}$ ergs/s (Markert and Clark 1975; Johnston et al. 1979). Considering the high luminosity of the source and pattern traced by it in CCD and HID, it was suggested that LMC X-2 probably belongs to the Z-Class (Smale and Kuulkers 2000). An extensive analysis of the data from the proportional-counter-array (PCA) onboard *Rossi-X-ray Timing Explorer (RXTE)* satellite revealed a complete Z-diagram of this source, making it the first extragalactic Z-source and seventh in this group (Smale et al. 2003). The source also exhibited 8.16 hours modulation in the X-ray lightcurve (Smale and Kuulkers 2000).

The *EXOSAT* spectra of this source in the $0.9-20$ keV band can be well fitted with either a thermal Comptonization model with temperature $\sim 3$ keV or a combination of a blackbody ($kT_{bb}\sim1.2$ keV) and thermal bremsstrahlung emission ($kT_{th}\sim5$ keV) (Bonnet-Bidaud et al. 1989). The *XMM-Netwon* X-ray spectrum of the source was well described by a model consisting of a blackbody emission from the neutron star surface and disc blackbody emission from the standard thin disc (Lavagetto et al. 2008). They also attempted with a Comptonization model to describe the X-ray spectrum of the source. During their observation, the source was in the normal branch.

Agrawal and Misra (2009) carried out a detailed spectral study of this source using *RXTE* and *Suzaku* data. They studied the evolution of the X-ray spectra along the complete Z-track using $3-20$ keV *RXTE-PCA* observations. They fitted the $3-20$ keV spectra with absorbed *compTT* model and found that the Comptonized component comes from an optically thick (optical depth $\tau\sim12$) and a cool corona (electron temperature $kT_e\sim1.9-2.7$ keV). They also suggested that a systematic variation in the Compton parameter $y$ is responsible for the motion of the source along the Z-track. They also fitted the *Suzaku* XIS + PIN data for both flaring and quiet state with two component models. They found that the combination of a disc blackbody and *compTT* components provides a better fit compared to the *bbody+compTT* model.

Till now no clear evidence of QPO feature has been found in this source. The power density spectra (PDS) of this source for all the three branches (HB, NB and FB) can be described by a simple power-law (Smale et al. 2003).

In this work, we present the results of the first *AstroSat* observations of the source LMC X-2. We have investigated the X-ray spectral evolution of the source LMC X-2 in the energy range of $0.5-20.0$ keV along the complete Z-pattern in the HID. This is the first such detailed study of this source. We have studied the evolution of the PDS along the three branches of the Z-pattern. The remainder of the paper is organized as follows. The observations and procedure of the data reduction is presented in §2. Method of data analysis and the modelling of the energy spectra and the power density spectra are presented in §3. The results of the spectral and temporal analysis are described in §4. Finally, we discuss the implications of our results and conclude in §5.

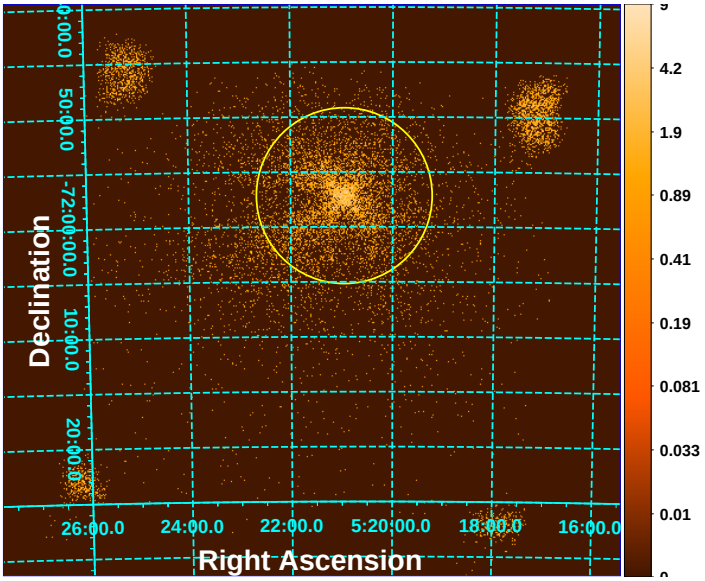



**Figure 1.** The image of LMC X-2 as observed by *SXT* in June 2016. The spectra and lightcurves have been extracted from a circular region of 8 arcmin as shown in the figure. The four spots seen at the corners of the image are calibration sources ($Fe^{55}$).

## 2 OBSERVATIONS AND DATA REDUCTION

*AstroSat* observed the source LMC X-2 from June 22, 2016 to June 24, 2016 using the instruments (*SXT* and *LAXPC*) onboard *AstroSat*, for a total exposure time of 140 ks. *AstroSat* provides an unique opportunity to understand the spectral and timing behaviour of a celestial source in $0.5-100$ keV with its suite of three co-aligned instruments: Soft X-ray Telescope (*SXT*, Singh et al. (2016)), Large Area X-ray Proportional Counter (*LAXPC*, see Yadav et al. (2016)) and Cadmium-Zinc-Telluride Imager (*CZTI*, Vadawale et al. (2016)). Here, we have used the data collected with the *SXT* and *LAXPC* instruments. *SXT* operates in the energy range $0.3-8.0$ keV and *LAXPC* operates in the $3.0-80.0$ keV band. During our observation, *SXT* was operated in the photon counting (PC) mode. The time resolution in this mode is 2.37 s. During our observation, *LAXPC* was operated in the event analysis mode in which events were tagged with an accuracy of 10 micro-seconds. *LAXPC* consists of three co-aligned identical X-ray proportional counters (LAXPC10, LAXPC20 and LAXPC30) with combined effective area of $\sim6000$ cm$^2$.

We used XSELECT version 2.4d to extract the image, lightcurves and spectrum from the *SXT* level2 event files provided by the instrument team. We used a circular region of 8 arcmin centered at the source position to extract the

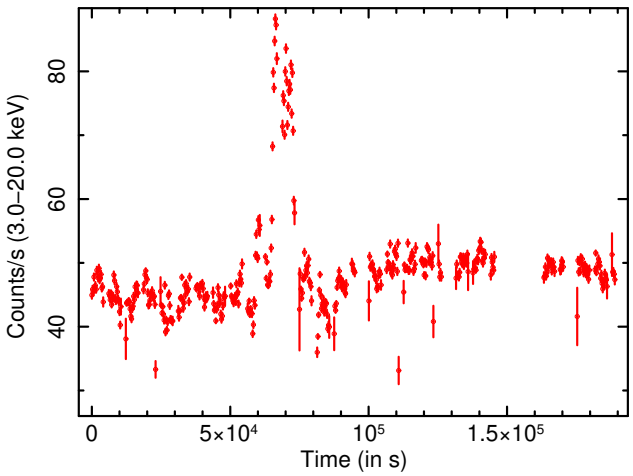



**Figure 2.** The background subtracted lightcurve of LMC X-2 in the energy range $3.0 - 20.0$ keV. The lightcurve is created using the LAXPC10 data. The time binsize used for the lightcurve is 256 s.

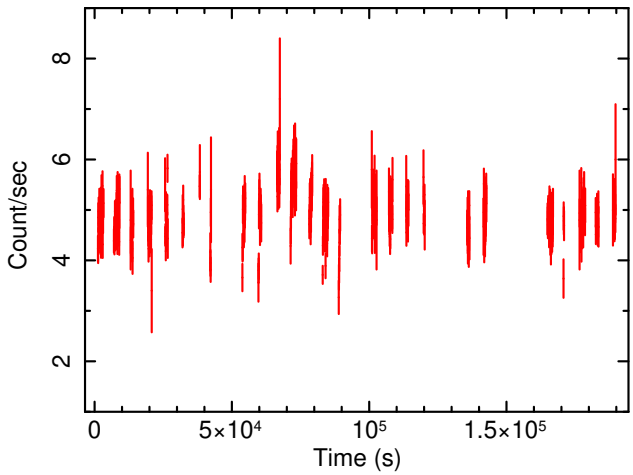



**Figure 3.** The background subtracted *SXT* lightcurve of LMC X-2 in the energy range $0.3 - 8.0$ keV. The time binsize used for the lightcurve is 64 s.

source spectrum and lightcurves. In Figure 1, we show the *SXT* image of the LMC X-2 for the Orbit number 3977. We created the instrument ARF using the tool *sxtmkarf* provided by instrument team [1], which also takes care of the off-pointing correction. We utilized the latest version of the software "LaxpcSoft" provided by the *LAXPC* team [2] to analyze the *LAXPC* data and followed the procedure described there (see also Agrawal et al. 2018; Sreehari et al. 2019).

## 3 DATA ANALYSIS

### 3.1 Lightcurve and Z-track

We used the top layer LAXPC10 event data to construct the lightcurve. Since above 20 keV the intensity is dominated by the contribution from the background, we created the lightcurve in the energy band of $3.0-20.0$ keV. In Figure 2, we show the background subtracted binned lightcurve in the energy range of $3.0 - 20.0$ keV. The binsize used here is 256 seconds. The source exhibited a flare during our observations. The background subtracted lightcurve created using *SXT* data is shown in Figure 3.

Hardness Intensity Diagram (HID) was created using the background subtracted lightcurves. We defined the overall colours as the ratio of count rates in the energy bands $6.5 - 18.5$ keV and $3.0 - 6.5$ keV, whereas intensity was defined as the total count rates in the $3.0 - 18.5$ keV energy band. We plotted the overall colours against the source intensity to construct the HID. The HID is shown in Figure 4. We used a binsize of 1024 s to create the HID. The large time binsize has been used here to separate the three branches of the Z-pattern. All the three branches of the Z-track can be identified clearly in the HID (Figure 4). The HID shows remarkable similarity with that obtained using the *RXTE* data (Smale et al. 2003; Agrawal and Misra 2009).

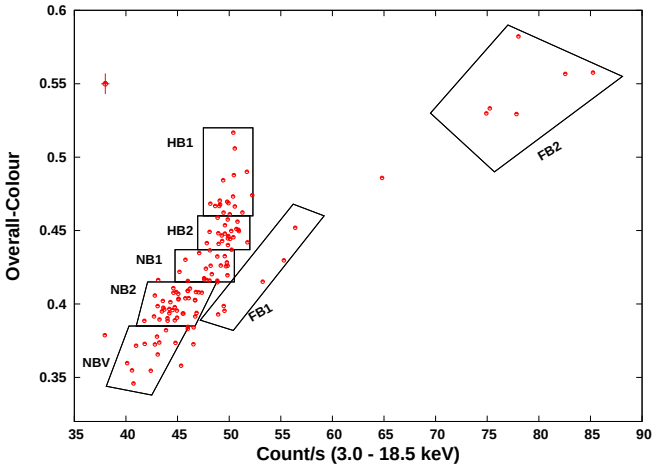



**Figure 4.** Hardness Intensity Diagram (HID) of LMC X-2 created using the LAXPC10 data. To create the HID, we have used 1024 s binsize. Different sections of the HID have been marked. A typical error bar on the data points is shown in the top-left corner. See text for details.

In order to study the evolution of the broadband spectral and temporal behaviour along the complete Z-track, we divided this track into 7 segments. We divided the horizontal branch (HB) into two sections 'HB1' and 'HB2'. The normal branch (NB) was also divided into two sections namely 'NB1', 'NB2'. The points close to the lower-most NB and the bottom part of the FB are part of the NB-FB vertex (NBV). The rest of the FB was divided into two sections 'FB1' and 'FB2'.

### 3.2 Spectral Analysis

We used the *LAXPC10* top layer data to create the source and background spectra for different sections of the HID. The latest *SXT* and *LAXPC* response matrix files provided by the instrument team were used for the spectral analysis. The sky background spectrum provided by the *SXT* team was used for the background subtraction. We used combined

[1] http://www.tifr.res.in/∼astrosat_sxt/dataanalysis.html
[2] http://www.tifr.res.in/∼astrosat_laxpc/LaxpcSoft.html

*SXT* (0.5 − 5.5 keV) and LAXPC10 (3.0 − 20.0 keV) data for spectral analysis. We restricted our analysis to these energy ranges because there is not enough source flux above 5.5 keV for the *SXT* and above 20 keV for the *LAXPC*. The combined spectra in the energy range 0.5 − 20 keV were fitted with the XSPEC version 12.9.1. We grouped the *SXT* data to give a minimum of 25 counts/bin. All the errors were computed using $\Delta\chi^2 = 1.0$ (68% confidence level). We added 1% systematics during fitting to account for the uncertainty in the response matrix.

According to the Dickey and Lockman survey, the galactic $N_H$ in the direction of LMC X-2 is $0.063 \times 10^{22}$ $cm^{-2}$ (Dickey and Lockman 1990). However, $N_H$ calculated using the more recent surveys like Leiden/Argentine/Bonn (LAB) (Kalberla et al. 2005) and HI4PI (Bailin et al. 2016) is $0.15 \times 10^{22}$ $cm^{-2}$. To calculate the $N_H$, we used the nH calculator tool provided by HEASARC, NASA. We used the multiplicative model *Tbabs* of XSPEC to account for the galactic absorption.

First, we fitted the spectra with a simple *cutoffpl+bbodyrad* model. This model has been used to describe the spectra of Z-sources (Birmingham model; see Jackson et al. 2009; Balucinska-Church et al. 2010). We found that for all parts of the Z-track photon index of the cutoff powerlaw was < 1. Hence *cutoff-powerlaw* is not consistent with the Comptonization model. We refer to this model as **Model 1**. We tried using other complex Comptonization models such as *nthComp*. The *nthComp* model has provision to select the blackbody or disc blackbody as the input seed photon spectrum (Zdziarski et al. 1996). Yet, another Comptonization model such as *compTT* which has been used previously to model the spectrum of this source (Lavagetto et al. 2008; Agrawal and Misra 2009) assumes a Wien spectrum for the seed photons (Titarchuk 1994). The model provided statistically good fit to the spectra of all the sections of the Z-track. We refer to this model as **Model 2**. We also tried a combination of disc blackbody (*diskbb*) and *nthComp*, as well as a combination of blackbody (*bbody*) and *nthComp* model. We noticed that addition of a *blackbody* or a *diskbb* component to the *nthComp* did not improve the fit. This suggests that, probably the disc is obscured by a Comptonized corona. The seed photons for the Comptonization may come from the obscured inner accretion disc or from the surface of the central source. Here, we assumed that the seed photons comes from the accretion disc. However, it is possible that the blackbody emission from the surface of the neutron star may also supply the seed photons for the Comptonization.

We also fitted the data with *diskbb+bbodyrad* model, which has been previously used to model the spectra of this source (Lavagetto et al. 2008) and the other LMXBs (Mitsuda et al. 1984). The above combination provided a poor fit compared to the *nthComp* model for the HB and NB sections (see Table 2 and Table 3). However, *diskbb+bbodyrad* and *nthComp* model gives similar reduced $\chi^2$ ($\chi^2/dof$) in the FB. We refer to this model as **Model 3**. In Figure 5, we show the residual resulted by fitting the spectra of the section HB2 with **Model 2** and **Model 3**. From the residual, it is clear that **Model 2** (bottom panel of Figure 5) is better compared to **Model 3** (top panel of Figure 5). While fitting the spectra with these models, we did not find any residual around $\sim 5-7$ keV range, suggesting that the iron line (Fe-K) feature is absent in this source during our observations.

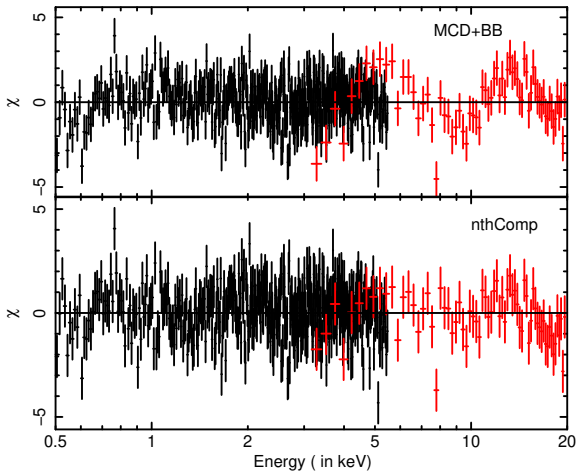



**Figure 5.** The residual in unit of sigma for *diskbb+bbodyrad* (MCD+BB) model (top panel) and *nthComp* model (bottom panel). From figure, it is clear that the *nthComp* model provides a better fit compared to the *diskbb+bbodyrad* model.

### 3.3 Timing Analysis

We used the LAXPC lightcurves in the energy range 3.0 − 20.0 keV to create the PDS. The lightcurves with binsize 4 ms were divided into intervals of 262144 bins, which allowed to study the nature of timing variabilities in the range of 0.001 − 125.0 Hz. PDS were created for each interval and those belonging to the same section of the HID are averaged. We rebinned the PDS in the frequency space by a factor of 1.3. The binned PDS were normalized to the fractional rms spectra (in units of $(rms/mean)^2 Hz^{-1}$) and an appropriate Poisson noise was subtracted (Zhang et al. 1995; Agrawal et al. 2018). To get a better statistics, we merged the PDS belonging to the same branch. While averaging the PDS for the NB branch, we assigned NBV data points as a part of the NB. PDS of all these three branches can be fitted with a simple power-law ($A\nu^{-\alpha}$). While fitting the PDS of FB with a power-law model, we found a signature of a weak QPO-like feature at $\sim 0.6 - 0.7$ Hz. Fitting this feature with an extra Lorentzian component improved the fit. The reduced $\chi^2$ decreased from 16.2/32 to 11.5/30.

## 4 RESULTS

### 4.1 Spectral Behaviour

The broadband spectra (0.5 − 20.0 keV) along the Z-track can be fitted with an absorbed Comptonization model (**Model 2**). We also tried the combination of emission from the multicolour disc (described by *diskbb* in XSPEC) and blackbody component (**Model 3**). We found that **Model 3** is not satisfactory for describing the spectra of the HB and the NB (see Table 3). The spectral parameters and reduced $\chi^2$ of **Model 2** and **Model 3** are given in Table 2 and Table 3 respectively. **Model 3** gave the inner disc temperature in the range of $\sim 0.8 - 1.0$ keV and black body temperature in the range of $1.5 - 1.8$ keV. In Figure 6, we show the spectra

**Table 1.** The best fit spectral parameters for **Model 1** (*Tbabs*(cutoffpl+bbodyrad)*). $\Gamma$ is photon index and $E_C$ is cutoff energy. $K$ is the normalization of the cutoff powerlaw at 1 keV and in units of $photons/s/cm^2/keV$. $N_{BB}$ is the normalization of the blackbody component and $kT_{BB}$ is its temperature. $N_H$ is in units of $10^{22}$ cm$^{-2}$.

| Parameters | HB1 | HB2 | NB1 | NB2 | NBV | FB1 | FB2 |
|---|---|---|---|---|---|---|---|
| $N_H$ | 0.065(fix) | 0.10±0.01 | 0.065(fix) | 0.065(fix) | 0.065(fix) | 0.065(fix) | 0.065(fix) |
| $\Gamma$ | 0.27±0.06 | 0.41±0.06 | 0.30±0.06 | 0.21±0.05 | 0.15±0.07 | -0.16±0.09 | -0.26±0.05 |
| $E_C$ (keV) | 2.94±0.08 | 2.97±0.08 | 2.75±0.06 | 2.54±0.05 | 2.38±0.06 | 2.20±0.06 | 2.58±0.05 |
| $K$ ($\times10^{-2}$) | 4.85±0.4 | 6.28±0.5 | 5.86±0.3 | 5.45±0.2 | 6.76±0.5 | 465.6±0.4 | 458±0.3 |
| $kT_{BB}$ (keV) | 0.42±0.01 | 0.37±0.01 | 0.39±0.01 | 0.39±0.06 | 0.31±0.02 | 0.33±0.01 | 0.36±0.01 |
| $N_{BB}$ | 350.0±32 | 515.0±50.5 | 390.1±37.5 | 445.2±32.1 | 1172.5±240.7 | 856.4±92.5 | 893.8±65.6 |
| $\chi^2/dof$ | 422/327 | 667/488 | 605/378 | 675/491 | 216/168 | 324/299 | 526/368 |

**Table 2.** The best fit spectral parameters for **Model 2** (*Tbabs*nthComp*). $kT_e$ and $kT_s$ are the electron temperature and seed photon temperature respectively. $\Gamma_C$ and $N_{Comp}$ are photon index and the normalization of *nthComp* component respectively. $\tau$ is the optical depth and $y$-par is the Comptonization parameter. $F_{Comp}$ is the $0.1-50$ keV unabsorbed Comptonization flux in units of ergs/s/cm$^2$. $N_H$ is the neutral hydrogen column density in untis of $10^{22}$ cm$^{-2}$. $L_X$ is $0.1-50$ keV unabsorbed luminosity in units of ergs/s.

| Parameters | HB1 | HB2 | NB1 | NB2 | NBV | FB1 | FB2 |
|---|---|---|---|---|---|---|---|
| $N_H$ | 0.17±0.02 | 0.22±0.02 | 0.16±0.02 | 0.16±0.01 | $0.08^{+0.06}_{-0.03}$ | 0.13±0.3 | 0.09±0.01 |
| $kT_e$ (keV) | 2.14±0.02 | 2.09±0.02 | 2.01±0.02 | 1.90±0.01 | 1.74±0.02 | 1.75±0.02 | 2.02±0.02 |
| $\Gamma_C$ | 1.85±0.01 | 1.87±0.01 | 1.87±0.01 | 1.87±0.02 | 1.77±0.02 | 1.71±0.01 | 1.61±0.01 |
| $kT_s$ (keV) | 0.38±0.05 | $0.27^{+0.05}_{-0.11}$ | 0.39±0.05 | 0.37±0.03 | 0.38±0.1 | $0.23^{+0.09}_{-0.07}$ | 0.32±0.06 |
| $N_{Comp}$($\times10^{-2}$) | 9.81±0.5 | $11.05^{+1.3}_{-0.6}$ | 10.5±0.3 | 9.87±0.3 | $9.27^{+2.1}_{-0.9}$ | 9.75±0.6 | 10.5±0.6 |
| $F_{comp}$ ($\times10^{-10}$) | 3.89±0.09 | 3.98±0.09 | 3.80±0.17 | 3.63±0.08 | 3.46±0.08 | 3.89±0.09 | 6.02±0.14 |
| $R_W$ (km) | 102±26.5 | 206.5±110.4 | 97.2±24.3 | 149.5±25.5 | 89.5±36.5 | 253.5±110.5 | 150.2±55.4 |
| $\tau$ | 13.35±0.16 | 13.31±0.15 | 13.65±0.3 | 14.05±0.31 | 15.97±0.41 | 16.77±0.24 | 17.15±0.28 |
| $y-par$ | 2.98±0.06 | 2.91±0.06 | 2.91±0.12 | 2.92±0.13 | 3.47±0.15 | 3.85±0.11 | 4.62±0.14 |
| $L_X$ ($\times10^{38}$) | 1.15±0.02 | 1.18±0.03 | 1.13±0.05 | 1.08± 0.02 | 1.03±0.02 | 1.15±0.03 | 1.79±0.04 |
| $\chi^2/dof$ | 415/327 | 663/489 | 604/378 | 675/491 | 197/168 | 309/299 | 484/368 |

of the HB2, NB2 and FB2 fitted with **Model 2**. The $N_H$ values derived using **Model 2** lie in the range of $(0.1-0.2)$ $\times\ 10^{22} cm^{-2}$. The derived $N_H$ values in the direction of LMC X-2 are close to the results of recent surveys (Kalberla et al. 2005; Bailin et al. 2016). Moreover, systematics in the data and model can also affect the best-fit values of $N_H$.

Fitting the spectra with **Model 2** gave the electron temperature in the range of $1.7-2.1$ keV (see Table 2). The electron temperature decreased as the source moved from the HB to the NB and then again increased as it moved up along the FB. The photon index of the Comptonized emission was around $\sim 1.85$ from the top-left HB to the lower NB. Then as the source moved down the NB-FB vertex (NBV) and then up in the FB the photon index decreased or the source spectrum became harder. We also computed the optical depth by formula given in Zdziarski et al. (1996) and the Comptonization parameter using a relation $y = \frac{4kT_e}{m_e c^2} max(\tau, \tau^2)$. The optical depth did not show significant change from HB1 to NB2 and remained in the range of $13.2-14.3$. As the source moved to the vertex (NBV), the optical depth increased from 14.05±0.31 to 15.97±0.41 and continued to increase along the FB. The Comptonization parameter $y$ decreased from $\sim 2.98$ to to $\sim 2.92$ as the source moved down the HB and then remained constant in the NB (NB1 and NB2). The $y$ parameter increased from 3.47±0.15 to 4.62±0.14 with the movement of the source from the vertex (NBV) to the FB2. Since the distance ($\sim 50$ kpc) to the source is known with a better accuracy (Freedman et al. 2001), the uncertainty in the intrinsic luminosity of the source is also much less compared to other Z-sources. The luminosity of the source showed a systematic decrease as the source moved from the upper NB to the vertex (NBV), and as the source further moved up the FB the luminosity increased. The luminosity varied in the range $(1.03-1.79)$ $\times10^{38}$ ergs/s. We show the evolution of the best fit spectral parameters of **Model 2** in Figure 7.

We also computed the the radius of the seed photon emitting region using the formula (see in 't Zand et al. 1999),

$$R_W = 3\times10^4 D \frac{\sqrt{\frac{f_{bol}}{1+y}}}{kT_s^2}. \quad (1)$$

The Wein radius $R_W$ was found to be in the range of $70-310$ km and did not show any clear correlation with the position on the Z-track (see Table 2). Here, $D$ is the distance to the source in kpc, $y$ is the Comptonization parameter and $f_{bol}$ is the bolometric $(0.1-50$ keV) flux of the Comptonized component.

We also derive the inner disc radius and the blackbody radius using the parameters of **Model 3**. The inner disc radius $R_{dbb}\sqrt{\cos\theta}$ is given by $\sqrt{N_{dbb}} D_{10}$, where $\theta$ is the inclination angle and $D_{10}$ is the distance to the source in the unit of 10 kpc. Similarly, the radius of blackbody emitting

**Table 3.** The best fit spectral parameters for **Model 3** (*Tbabs*(diskbb + bbodyrad)*. $kT_{bb}$ is the blackbody temperature and $kT_{in}$ is the inner disc temperature. $N_{bb}$ and $N_{dbb}$ are the normalization of the *bbodyrad* and *diskbb* components respectively. $N_H$ is in units of $10^{22}$ $cm^{-2}$.

| Parameters | HB1 | HB2 | NB1 | NB2 | NBV | FB1 | FB2 |
|---|---|---|---|---|---|---|---|
| $N_H$ | **0.09±0.01** | 0.09±0.01 | 0.10±0.006 | 0.063(fixed) | 0.07±0.01 | 0.063(fixed) | 0.063(fix) |
| $kT_{in}$ (keV) | 0.97±0.02 | 0.88±0.01 | 0.93±0.02 | 0.84±0.02 | 0.87±0.02 | 0.81±0.02 | 0.92±0.01 |
| $N_{dbb}$ | 19.42±1.92 | 29.71±1.85 | 22.91±2.07 | 32.29±2.04 | 28.48±3.36 | 35.27±4.12 | 27.35±1.65 |
| $kT_{bb}$ (keV) | 1.80±0.02 | 1.72±0.01 | 1.71±0.01 | 1.60±0.01 | 1.54±0.01 | 1.51±0.01 | 1.79±0.01 |
| $N_{bb}$ | 2.21±0.11 | 2.70±0.10 | 2.71±0.13 | 3.32±0.13 | 4.35±0.24 | 4.87±0.26 | 4.56±0.15 |
| $R_{dbb}\sqrt{\cos\theta}$ (km) | 22.03±1.08 | 27.25±0.85 | 23.95±1.08 | 28.42±0.89 | 26.68±1.58 | 29.70±1.72 | 26.15±0.78 |
| $R_{bb}$ (km) | 7.43±0.18 | 8.21±0.15 | 8.23±0.19 | 9.09±0.18 | 10.42±0.28 | 11.03±0.29 | 10.67±0.17 |
| $\chi^2$/dof | 440/327 | 759/489 | 651/378 | 705/491 | 211/168 | 307/300 | 481/369 |

**Table 4.** The best fit parameters obtained by fitting the PDS of different branches of the Z-track. $\alpha$ is the index and $A$ is the normalization of the power-law component. Pow-rms is the total rms of the power-law component in the frequency range $0.001 - 50$ Hz and QPO-rms is the rms of the QPO feature in the frequency range $0.001 - 50$ Hz.

| Parameters | HB | NB | FB |
|---|---|---|---|
| $\alpha$ | 1.70±0.22 | 0.83±0.12 | 1.71±0.11 |
| $A(\times 10^{-5})$ | 0.078±0.03 | 13.4±2.5 | 0.87±0.3 |
| Pow-rms (%) | 1.21±0.82 | 3.61±1.62 | 3.97±1.58 |
| $\nu_c$ (Hz) | | | 0.65±0.07 |
| $FWHM$ (Hz) | | | 0.2 (fixed) |
| LN ($\times 10^{-3}$) | | | 2.48±0.84 |
| QPO-rms (%) | | | 2.71±0.52 |
| F-test | | | $5.8 \times 10^{-3}$ |
| $\chi^2$/dof | 27.1/32 | 26.2/32 | 11.5/30 |

region is given by $\sqrt{N_{bb}}D_{10}$. The inner disc radius is found to be in the range of $20 - 30$ km and the blackbody radius varies in the range of $7 - 11$ km.

### 4.2 Power-spectral Properties

We detected very low-frequency noise (VLFN) in all the three branches (HB, NB and FB). For the NB, we found index $\alpha = 0.83\pm0.11$ and integrated rms ($0.001 - 50$ Hz) $= 3.61\pm1.62\%$. The VLFN in the HB has integrated rms $= 1.21\pm0.82\%$ and that in the FB has integrated rms $= 3.97\pm1.58\%$. We found a marginal evidence of QPO at $0.65\pm0.07$ Hz in the FB with significance $\sim 2.8\ \sigma$ and integrated rms ($0.001 - 50$ Hz) $= 2.71\pm0.52\%$. The best fit PDS model parameters for HB, NB and FB are presented in Table 4. Figure 8 shows the PDS for these three branches along with the best fit model.

## 5 DISCUSSION

The bright low-mass X-ray binary LMC X-2 traced a complete Z-track during the $\sim$ 140 ks *LAXPC* observations. We also note that the range of the overall color values ($0.3 - 0.6$) during our observations is similar to that observed during the *RXTE* observations (Smale et al. 2003; Agrawal and Misra 2009). The track in the HID is almost identical during the *RXTE* and the present *AstroSat* observations. We also note that the source spent $\sim$ 12 ks or 8% time in the flaring state. Using these observations, we studied the evolution of the broadband ($0.5 - 20$ keV) spectral parameters along the complete Z-track by combining the *SXT* and *LAXPC* data, which is a first such study. Previously, spectral evolution of the source has been investigated along the Z-track using the data from the *RXTE-PCA* in the energy range of $3.0 - 20.0$ keV (Agrawal and Misra 2009).

Here, we have shown that the $0.5 - 20.0$ keV spectra of the source can be described by a simple absorbed Comptonization model (**Model 2**). We find that the Comptonizing region is cool and optically thick with the electron temperature in the range of $\sim 1.7 - 2.1$ keV and the optical depth in the range of $\sim 13.2 - 17.5$. The *RXTE-PCA* spectra in the $3.0 - 20.0$ keV energy band, fitted with *compTT* model provided a similar optical depth ($\tau \sim 13.0 - 18.0$) but a slightly higher electron temperature ($kT_e \sim 1.95 - 2.7$ keV) (Agrawal and Misra 2009).

Most importantly, we do not require an extra disc emission component or a blackbody component to fit the spectra in the $0.5 - 20.0$ keV range unlike *Suzaku* observations (Agrawal and Misra 2009). It is worth mentioning that the $0.3 - 10.0$ keV *XMM-Newton* spectrum of the source was also modeled using a pure Comptonized emission (Lavagetto et al. 2008). The possible explanation for the absence of the soft component is that the temperature of the soft component may be well below the lower energy bound of the instrument, considered while fitting. The seed photon temperature $kT_s$ in our case is $\sim 0.2 - 0.4$ keV. However, a significantly lower value of $kT_s$ ($\sim$ 40 eV) has

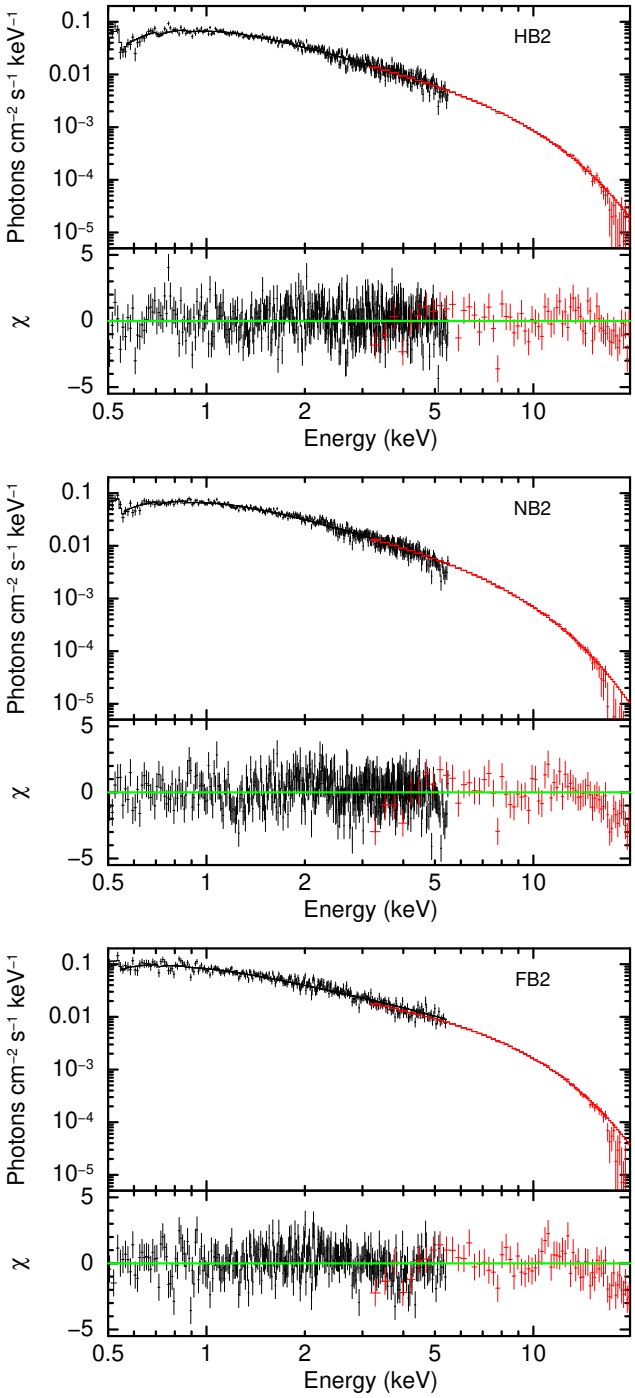



**Figure 6.** The unfolded spectra at different parts (HB2, NB2, FB2) of the Z-track along with the residual (bottom panels) in the units of sigma.

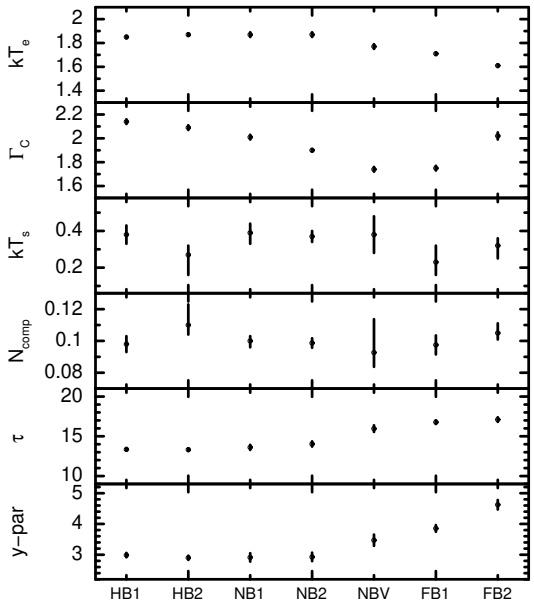



**Figure 7.** The evolution of the best fit spectral parameters of **Model 2** along the Z-track. $y-par$ (Comptonization parameter) and $\tau$ (optical depth) are derived parameters (see text for details).

been reported by Lavagetto et al. (2008) using the *XMM-Newton* observation. They also calculated the radius of seed photons emitting region and it was found to be very high ($R_W \sim 10^4$ km) and which lead to conclusion that Comptonization model is not physically acceptable. In our case, the radius of seed photon emitting region is $70 - 310$ km and hence the Comptonization model (*nthComp*) is an appropriate to represent the spectra of the source along the Z-track.

We have studied the evolution of the spectral parameters along the Z-tarck. Though variations in these parameters are subtle, they provide an important probe to understand the movement of the source along the Z-pattern. Our findings suggest that the optical depth of the corona increases as the source moves from the NB-FB vertex (NBV) to the upper FB. We also note that the Compton $y$ parameter also increases along the FB. This trend is also seen in other Z-sources (GX 349+2: Agrawal and Sreekumar 2003, GX 17+2: Agrawal et al. 2020) and in the previous observations of LMC X-2 (Agrawal and Misra 2009). The observed variations in the spectral parameters ($\tau$ and $y$) suggest that most probably at the vertex of the NB and the FB, the accretion rate crosses the Eddington limit and a strong radiation pressure drives a fraction of the disc material into a hot central corona. The above scenario has been discussed by Agrawal and Sreekumar (2003); Agrawal et al. (2020) to explain the increase of the optical depth along the FB in the Z-sources GX 349+2 and GX 17+2. Hence, the motion from the vertex to the upper FB can be understood in terms of increasing accretion rate scenario.

It has been observed that in some of the Z-sources the optical depth of the Comptonized component generally decreases as the source moves from the HB to the lower NB (GX 17+2: Di Salvo et al. 2000; Agrawal et al. 2020, GX 349+2: Agrawal and Sreekumar 2003, GX340+0: Iaria et al. 2006, Cyg X-2: Di Salvo et al. 2002) and the electron temperature either remains constant (Agrawal et al. 2020; Di Salvo et al. 2000) or increases (Di Salvo et al. 2002; Agrawal and Sreekumar 2003; Iaria et al. 2006). In the present case, the electron temperature of the Comptonizing region decreases as the source moves from HB to the vertex of the NB and FB. However, the optical depth remains nearly constant upto the middle of NB (NB2). The source exhibited a similar behaviour during the *RXTE* observations (Agrawal and Misra 2009). The decrease in the

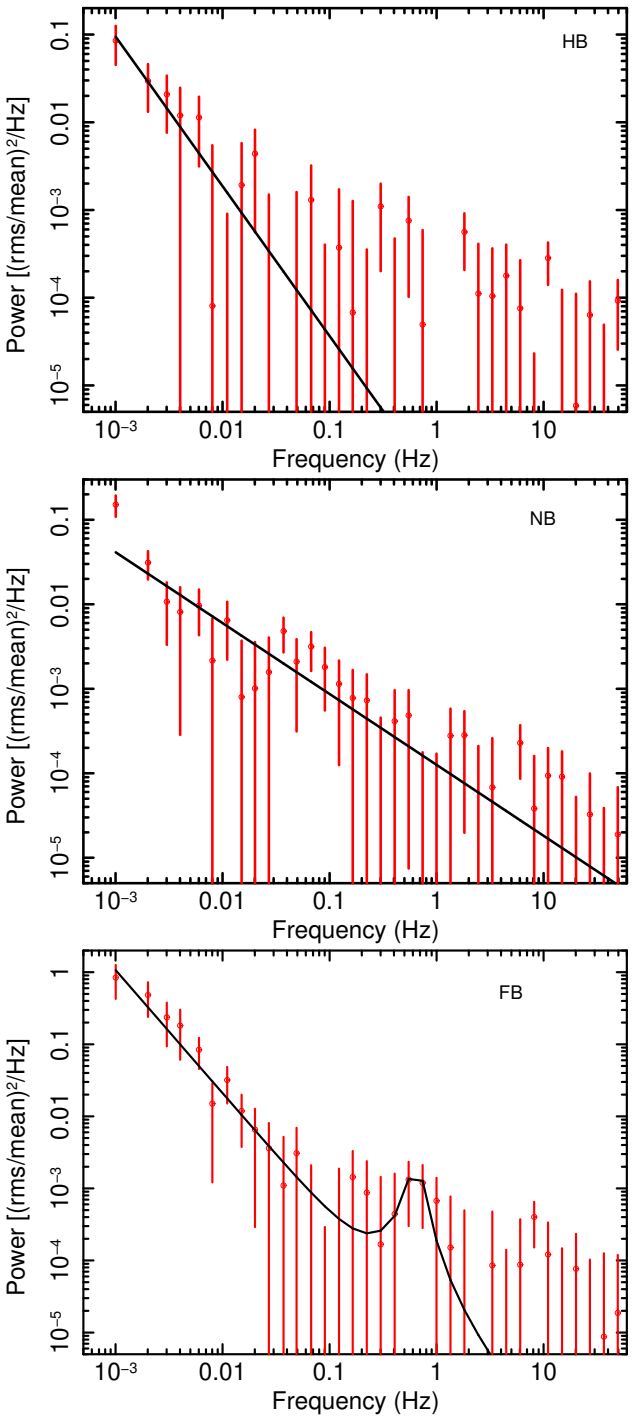



**Figure 8.** Power density spectra (PDS) for different branches (HB, NB, FB) of the Z-track along with the best fit Model. Marginal detection of QPO-like feature is seen in FB. See, text for details.

$kT_e$ can be explained in terms of cooling of the corona due to increase in the seed photon supply. However, it is also possible that a part of the coronal material cools down and settles in the disc causing the optical depth to decrease and the temperature of the remaining material in the corona will either not change or will increase. The above scenario can explain the spectral behaviour of other Z-sources.

We have derived PDS for the three branches (HB, NB and FB). In all three branches, PDS has the VLFN component. Smale et al. (2003) found VLFN component with $\alpha \sim 0.60$ in the HB, $\alpha \sim 0.90$ in the NB and $\alpha \sim 1.33$ in the FB. In our case, the VLFN in the HB and FB is steeper compared to the previous results (Smale et al. 2003). However, the value of VLFN index in the NB is close to that obtained by Smale et al. (2003). We also detect a weak ($\sim 2.8\ \sigma$) QPO at $\sim 0.65$ Hz in the FB. The rms amplitude of the QPO is $\sim 2.7\%$.

## ACKNOWLEDGEMENTS

Authors thank the anonymous reviewer for providing useful suggestions which improved the quality of the manuscript. This research has made use of the data obtained through GT phase of *AstroSat* observation. Authors thank DD, PDMSA and Director, URSC for encouragement and continuous support to carry out this research. Authors also thank Ravishankar B. T. of SAG for careful reading the manuscript and providing useful comments. This work has used the data from the LAXPC Instruments developed at TIFR, Mumbai and the LAXPC POC at TIFR is thanked for verifying and releasing the data via the ISSDC data archive. We thank the AstroSat Science Support Cell hosted by IUCAA and TIFR for providing the LaxpcSoft software which we used for LAXPC data analysis. This work has used the data from the Soft X-ray Telescope (*SXT*) developed at TIFR, Mumbai, and the *SXT* POC at TIFR is thanked for verifying & releasing the data and providing the necessary software tools.

## DATA AVAILABILITY

Data underlying this article are available at *AstroSat*-ISSDC website (http://astrobrowse.issdc.gov.in/astro_archive/archive).

## REFERENCES

Agrawal V. K., Nandi Anuj, Ramadevi M. C., 2020, Ap&SS, 365, 41
Agrawal V.K., Nandi Anuj, Girish V., Ramadevi M.C., 2018, MNRAS, 477, 5437
Agrawal V.K., Misra R., 2009, MNRAS, 398, 1352
Agrawal V.K., Sreekumar P., 2003, MNRAS, 346, 933
Bailin J., Calabretta M.R., Dedes L., Ford H.A., Gibson B.K., Haud U., Janowiecki S., Kalberla P.M.W. et al., 2016, A&A, 594, A116
Balucinska-Church M., Gibbec A., Jackson N.K., Church M.J., 2010, A&A,512, A9
Bhulla Y., Misra R., Yadav J.S. et al.,2019, RAA, 19, 114
Bonnet-Bidaud J.M., Motch C, Beuermann K., Pakull M., Parmar A.N., van der Klis M., 1989, A&A, 213, 97
Cackett E.M., Miller J. M., Ballantyne D. R., Barret D., Bhattacharyya S., Boutelier M., Miller M.C., Strohmayer T. E., 2010, ApJ, 720, 205
Church M.J., Gibiec A., Balucinska-Church M., Jackson N.K., 2012, A&A, 546, A35
Dickey J.M., Lockman F.J., ARA&A, 1990, 28, 215

Di Salvo T. et al., 2002, A&A, 386, 535
Di Salvo T., et al., 2001,ApJ, 554, 49
Di Salvo T., Stella L., Robba N.R., van der Klis M., Burderi L., Israel G.L, Homan J., Compana S. et al., 2000, ApJ, 544, L119
Done C., Zycki P.T. and Smith D.A, 2002, MNRAS, 331, 453
Farinelli R., Paizis A., Landi R., and Titarchuk L.,2009, A&A, 498, 509
Freedman W.L., Madore B.F., Gibson B.K. et al., 2001, ApJ, 553, 47
Hasinger G., van der Klis M., 1989, A&A, 225, 79
in 't Zand, J.J.M., Verbunt F., Strohmayer T.E., Bazzano A., Cocchi M., Heise J., van Kerkwijk M.H., Muller J.M., et al., 1999, A&A, 345, 100
Iaria R., Lavagetto G., Di Salvo T., D' Ai A., Burderi L., Stella L., Robba N. R., 2006, Chin. J. Astron. Astrophys., 6, 257
Jackson N.K., Church M.J., Balucinska-Church M., 2009, A&A, 494,1059
Johnston M.D., Bradt H.V., Doxsey R.E., 1979, ApJ, 233 514
Kalberla P.M.W., Burton W.B., Hartmann D., Arnal E.M., Bajaja E., Morras R., Poppel W.G.L, 2005, A&A 440, 775
Lavagetto G., Iaria R., D'Ai A., Di Salvo T., Robba N. R., 2008,A&A, 478,181
Lin D., Remillard R.A., Homan J., Barret D., 2012, ApJ, 756, 34
Markert T.H., Clark G.W., 1975, ApJ, 196, L55
Pakull M., 1978, IAU Circular, 3313
Singh, K.P, Stewart G.C., Chandra S., Mukerjee K., Kotak S., Beardmore, A.P., Chitnis V., Dewangan G.C., et al., 2016, SPIE, 99051E, 10
Smale A.P., Kuulkers E., 2000, ApJ 528, 702
Smale A.P., Homan J., Kuulkers E., 2003, ApJ, 590, 1035
Mitsuda K., et al., 1984, PASJ, 36, 741
Titarchuk L., 1994, ApJ, 434,570
Vadawale, S.V., Rao A.R., Bhattacharya D., Bhalerao Varun B., Dewangan G.C., Vibhute A.M., Mithun N.P.S., Chattopadhyay T., et al, 2016, SPIE, 9905, 11
van der Klis M., 2000, ARA&A, 38, 717
Yadav J.S., Agrawal P.C., Antia H.M., Chauhan Jai Verdhan, Dedhia Dhiraj, Katoch Tilak, Madhwani P., Manchanda R.K, et al., 2016, SPIE, 9905, 15
Zdziarski A. A., Johnson W.N., Magdziarz P., 1996, MNRAS, 283, 193
Zhang W., Jahoda K., Swank J.H., Morgan E.H. and Giles A.B., 1995, ApJ, 449, 930